International Journal of Heat and Mass Transfer 144 (2019) 118608

Contents lists available at ScienceDirect

International Journal of Heat and Mass Transfer

journal homepage: www.elsevier.com/locate/ijhmt

Interface diffusion-induced phonon localization in two-dimensional lateral heterostructures

Yuxiang Ni [a,*], Honggang Zhang [a], Song Hu [a], Hongyan Wang [a], Sebastian Volz [b,c], Shiyun Xiong [d,*]

[a] School of Physical Science and Technology, Key Laboratory of Advanced Technologies of Materials, Ministry of Education of China, Southwest Jiaotong University, 610031 Chengdu, PR China
[b] Laboratoire EM2C, CNRS, CentraleSupélec, Université Paris-Saclay, Grande Voie des Vignes, 92295 Châtenay-Malabry Cedex, France
[c] LIMMS/CNRS-IIS(UMI2820) Institute of Industrial Science, University of Tokyo 4-6-1 Komaba, Meguro-ku, 153-8505 Tokyo, Japan
[d] Functional Nano and Soft Materials Laboratory (FUNSOM) and Collaborative Innovation Center of Suzhou Nano Science and Technology, Soochow University, 215123 Suzhou, PR China

ARTICLE INFO

Article history:
Received 24 May 2019
Received in revised form 4 August 2019
Accepted 20 August 2019
Available online 27 August 2019

Keywords:
Phonon localization
Interface diffusion
Molecular dynamics
Two-dimensional heterostructures

ABSTRACT

We report that the interface composition diffusion, which often occurs in the synthesis of two-dimensional lateral heterostructures, can significantly suppress the thermal transport property. Our molecular dynamics simulations show that the thermal conductivity of graphene/h-BN lateral heterostructures can be largely tuned by varying the interface composition diffusion length. The underling mechanism is explained by Anderson localization of phonons, which is corroborated by the exponential decay of the phonon transmission with composition gradient length. Phase breaking interactions are shown to delocalize the modes at elevated temperatures. The findings in this work suggest that composition graded interfaces can be used to tune the thermal transport of heterostructures via phonon localization, which is important for their applications in electronics, thermoelectrics and thermal insulators.

1. Introduction

Two-dimensional (2D) materials such as graphene, hexagonal boron nitrides (h-BN), and transition metal dichalcogenides (TMDs, e.g., MoS_2) have intrigued experimental and theoretical workers for their exceptional electrical, thermal, and optical properties. These different 2D materials can be integrated into lateral 2D heterostructure. The resulting artificial 2D structures provide access to new properties and applications beyond their component 2D atomic crystals and therefore, they are emerging as a new exciting field of research [1].

The synthesis of 2D lateral heterostructures has achieved significant progress in recent years [2–15]. The composition diffusion at the interface, which can cause nonabrupt, graded boundaries, is a key issue of interface formation in conventional heterostructures as well as their monolayer analogs [4]. Notably, compositional transition is often reported at the interface of these 2D heterostructures, which is typically in the range of 1∼35 nm. Liu et al. [5] demonstrated the creation of graphene and h-BN (Gr/h-BN) in-plane heterostructures by using lithography patterning and sequential chemical vapour deposition (CVD) growth steps. The sharpness of lateral interface between the h-BN and graphene layers was observed to be within 1 nm. Levendorf et al. reported the synthesis of Gr/h-BN lateral heterostructures with a patterned regrowth technique [6]. The obtained heterojunction has a compositional transition width of no more than 10 nm. Sutter et al. [4] report that high-temperature growth leads to intermixing near the interface of Gr/h-BN lateral heterostructures, similar to interfacial alloying in conventional heterostructures. Duan et al. [7] designed a thermal CVD process to synthesis WS_2-WSe_2 lateral heterostructures. The junction shows a transition from WS_2 to WSe_2 phases over a length scale of 35 nm. Slight inter-diffusion of transition-metal elements is also often observed along the armchair interfaces of WS_2 and MoS_2 lateral heterostructures, typically over a width of 1–3 unit cells [8].

There are several factors that lead to the composition-graded interface, including the temperature of the growth [4], the switching rate of the vapour-phase reactants and (or) ion diffusion across the interface [7], and the edge stability during the epitaxial growth [8], etc. The Gr/h-BN interface can even be tuned from comparatively sharp to graded by controlling the duration of a preheating period of the BN source [10]. While clean and sharp interfaces of 2D heterostructures are essential for preserving their optoelectronic properties [8], composition graded interface may have significant impact on the heat transport of 2D heterostructures. Unfortunately, little is known about the thermal property of 2D

* Corresponding authors.
E-mail addresses: yuxiang.ni@swjtu.edu.cn (Y. Ni), syxiong@suda.edu.cn (S. Xiong).

https://doi.org/10.1016/j.ijheatmasstransfer.2019.118608
0017-9310/

heterostructures with composition-graded interfaces, which is urgently needed for evaluating their potentials in the applications of electronics and thermoelectrics.

In this work, we report that the interface composition diffusion, even with a width of several nanometers, can significantly hinder the thermal transport property of Gr/h-BN lateral heterostructures. Our molecular dynamics (MD) simulations show that the thermal conductivity κ of Gr/h-BN heterostructures can be largely tuned by the interface composition diffusion length. Phonon localization is identified to be the cause of heat transfer suppressing in such structures at room temperature. The findings in this work suggest that introducing nonabrupt, graded interface to materials can be beneficial for their applications in thermoelectrics and thermal insulators, where low thermal conductivity is desired.

2. Method

2.1. Models

We started from a 4.2 $\times$ 111.2 nm Gr/h-BN lateral heterostructure with an abrupt interface. The interface was built with C-B zigzag linking edges in our models, since the zigzag edges were reported to be more preferably formed than the armchair counterparts [9]. The C—C, C—B, and B—N bond lengths were all set as 1.42 Å in the simulation with a lattice mismatch of $\sim$2.1% for h-BN, which has negligible effects on its thermal properties [16–18]. The structures with composition-graded interfaces were then generated by randomly switching the C (B/N) atoms by their B/N (C) counterparts across the interface. Within a distance L, the number of atoms ratio for C:B/N gradually decreases from 90%:10% to 10%:90%, as shown in Fig. 1(a). We studied the systems where L equals 8 nm, 16 nm and 24 nm, respectively. Here we define L as the compositional transition width. At the same composition proportion, the heterogeneous atoms (for example, carbon atoms in h-BN matrix) can appear individually, alternatively, several C atoms can aggregate and form a "particle". Thus in our study, models with four different sizes of the heterogeneous particles in the composition grading were built, each respectively consists of one, two, six and ten atoms (Fig. 1(b)).

Models shown in Fig. 1 were used in the non-equilibrium MD (NEMD) simulations, for the phonon transmission spectra calculations. Because of the non-linear temperature gradient in the composition graded structures, it is difficult to obtain the thermal conductivity (κ) from the direct method in NEMD. We thus resort

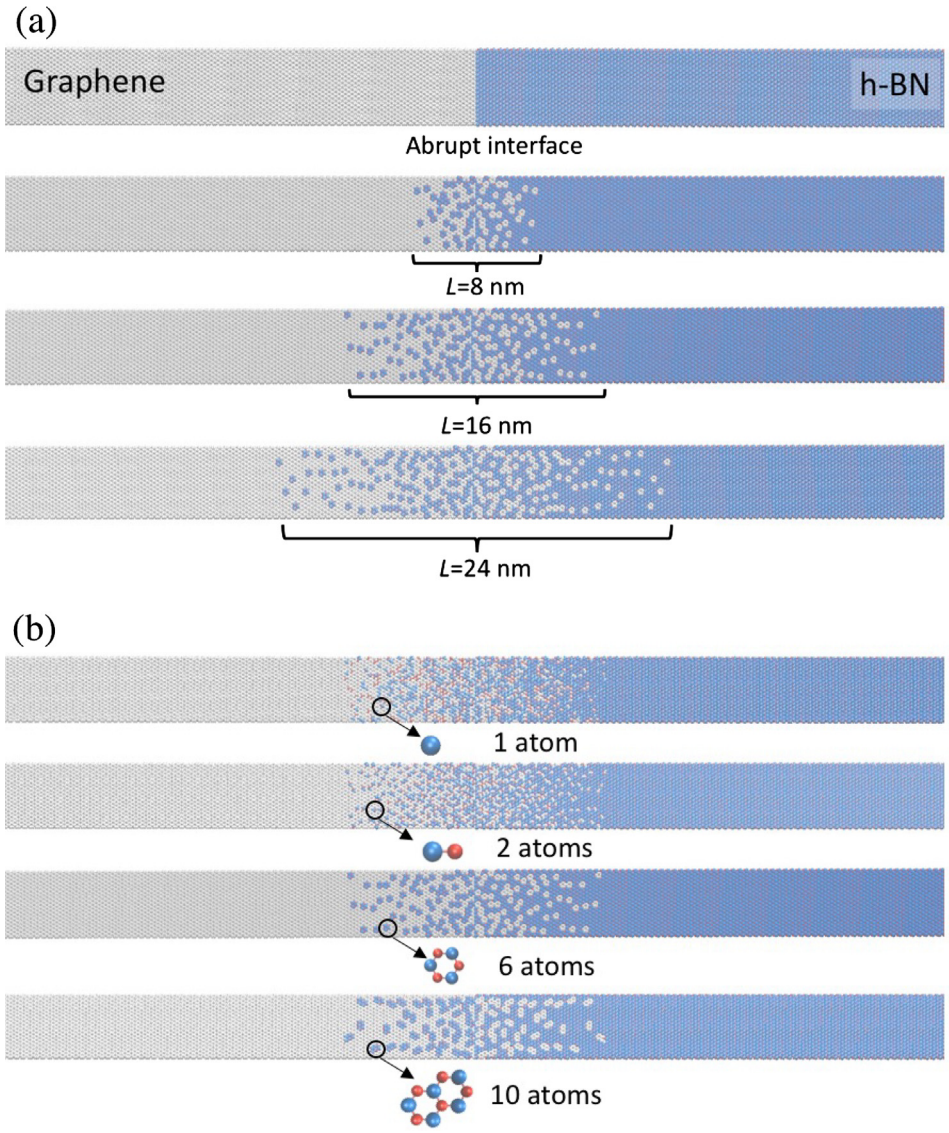

Fig. 1. (a) Structures of Gr/h-BN lateral heterostructure with abrupt interface and composition-graded interfaces with different compositional transition width L. The heterogeneous particle shown here consists six atoms; (b) Illustration of different sizes of the heterogeneous particles.

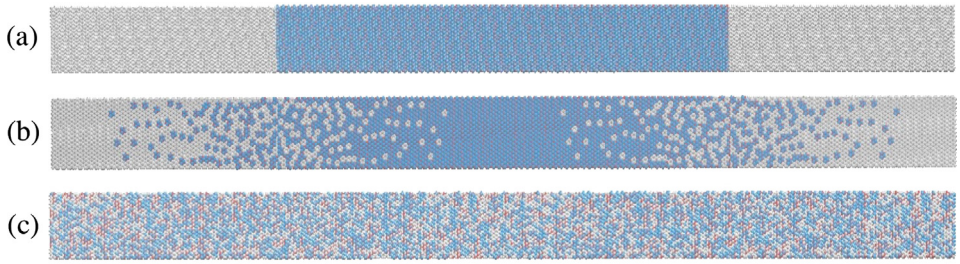

Fig. 2. Models used in the thermal conductivity calculations in EMD: (a) Gr/h-BN heterostructure with abrupt interfaces. (b) Gr/h-BN heterostructure with composition graded interfaces. In this model L equals 24 nm and the heterogeneous particle consists six atoms. (c) BNC hexagonal structures with random composition distributions.

to equilibrium MD (EMD) simulations and the Green–Kubo method.

In preparation for the thermal conductivity calculations, we horizontally flipped the models shown in Fig. 1 and combined them with the original ones, as illustrated in Fig. 2. This allows for applying a periodic boundary condition perpendicular to the interfaces, which is required by the Green–Kubo method. Each model contains two Gr/h-BN interfaces. The length of the models is 68 nm. BNC hexagonal structures with random composition distributions were also generated for comparison. We adopted the Tersoff potential to describe the BNC atomic interactions in our systems with parameters given in Ref. [19], which provides comparable phonon dispersion relation and thermal conductivity of both graphene and h-BN to the measured values [20–23].

2.2. Thermal conductivity calculation of Gr/h-BN lateral heterostructures

The initial structures shown in Fig. 2 were relaxed using a conjugate gradient energy minimization algorithm. Periodic boundary conditions were used in all directions. To mimic the free-stand structures, a vacuum of 20 nm is used in the direction perpendicular to the sheets. The MD time step was set to 0.5 fs. An MD run of 200 ps in the canonical ensemble (NVT) was performed to impose a temperature of 300 K. Then, the microcanonical ensemble (NVE) was applied for another 200 ps to achieve thermal equilibrium. Finally, the instantaneous heat fluxes along the armchair axis $j_A(t)$ were collected from MD runs with lengths equal to 2 ns. The Green–Kubo formula [24] was used to evaluate the thermal conductivity (κ_A) along the armchair direction:

$$\kappa_A = \frac{V}{k_B T^2}\int_0^{+\infty}\langle j_A(t) j_A(0)\rangle\, dt, \tag{1}$$

where k_B is the Boltzmann constant, T the temperature, and V the system volume. The angular brackets denote the ensemble average, performed here over twenty independent MD simulations.

2.3. Phonon transmission calculations

To quantitatively clarify the respective role of phonon scattering mechanisms, we calculated the composition transition width (L) dependent phonon transmission functions (T(ω)) from NEMD. T(ω) was calculated based on the method developed by K.Saaskilahti et al. [25,26]. The frequency resolved heat flux between any atom $i$and $j$can be expressed as:

$$q_{i\to j}(w) \approx -\frac{2}{t_{simu}\omega}\sum_{\alpha,\beta\in\{x,y,z\}} Im\langle \hat{v}_i^{\alpha}(\omega) * K_{ij}^{\alpha\beta}\hat{v}_j^{\beta}(\omega)\rangle, \tag{2}$$

where t_{simu} and ω are the simulation time and the frequency, respectively. $\hat{v}_i^{\alpha}(\omega)$ and $\hat{v}_j^{\beta}(\omega)$ are the Fourier transformed atomic velocities of atom i in direction α and atom j in direction β, respectively. For calculating the flux spectra, the force constant matrix is calculated with the finite displacement method by LAMMPS, i.e., after relaxing the structures to the potential minimum, atom i is moved in the directions $\pm x, \pm y, and \pm z$ with a small value (Δ = 0.01 Å). After each displacement, the forces F of each atoms are calculated. As a result, the element of the force constant matrix can be evaluated as:

$$K_{ij}^{\alpha\beta} = \frac{F_j^{\beta-} - F_j^{\beta+}}{2\Delta} \tag{3}$$

Here $F_j^{\beta-}$ and $F_j^{\beta+}$ denote the force on atom j in β direction when atom i is displace to -α and +α directions, respectively.

The heat current across any interface separating adjacent atom sets L and R can be obtained by summing over atoms in each set:

$$q(w) = \sum_{i\in L}\sum_{j\in R} q_{i-j}(\omega). \tag{4}$$

The phonon transmission function can thus be defined according to the spectral heat current as:

$$T(w) = \frac{q(w)}{k_B \Delta T}, \tag{5}$$

where ΔT is the temperature difference of the two thermal baths in NEMD simulations.

The atoms at the two ends of the structures shown in Fig. 1 are fixed. The atoms located within the distance L_{bath} = 30 nm from left and right adjacent to fixed areas are coupled to hot and cold Langevin heat baths at temperatures $L + \Delta T/2$ and $L - \Delta T/2$, respectively. The MD time step was set to 0.5 fs, and the coupling time constant of the Langevin thermostat was chosen as τ_{time} = 1 ps. The mean thermal bath temperature was fixed as T = 300 K, and ΔT was set as 60 K.

3. Results and discussion

3.1. Thermal conductivity of Gr/h-BN lateral heterostructures

Fig. 3 shows the calculated thermal conductivity of Gr/h-BN with different composition diffusion lengths and different sizes of heterogeneous particles. The κ of Gr/h-BN with abrupt interfaces is calculated as 324 W/mK, and the structures with composition graded interfaces clearly possess much lower κ. In general, κ decreases against L for all the models, indicating that the composition transition width is an influential factor in tuning the thermal transport property. This result can be understood as that when the spatial extent of the composition diffusion is larger, phonon scattering will occur in a broader spatial range along the structure and results in a shorter phonon mean free path, which is corroborated in the next section. Similar phenomenon was observed in SiGe superlattice nanowires with composition graded interfaces [27]. Note that κ of the BNC hexagonal structures with random

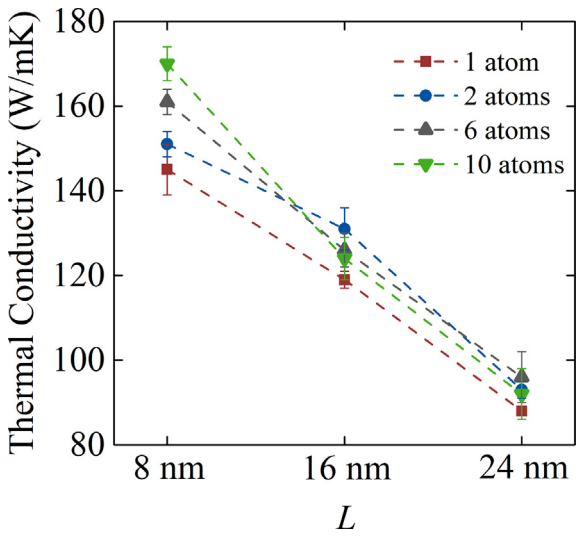

Fig. 3. Thermal conductivities of composition graded Gr/h-BN with different L and different sizes of heterogeneous particles. Note that κ of the corresponding structures with abrupt interfaces is 324 W/mK.

composition distributions is calculated as 58 W/mK, indicating the lower limit of κ in Gr/h-BN lateral heterostructures.

At L = 8 nm, the size of the heterogeneous particle has obvious impact on κ: smaller particles lead to lower κ. It can be seen from Fig. 1(b) that at the same position along the structure, smaller heterogeneous particles are more scattered, which leads to a greater chance for phonon scattering. Indeed, the phonon mean free path of graphene with h-BN domains was reported to decrease with decreasing domain size [28]. As L increases, the particle size impacts κ less because L predominates the κ reduction.

3.2. Phonon analysis and Anderson localization in Gr/h-BN lateral heterostructures

Fig. 4 depicts the composition transition width-dependent phonon transmission spectra at 300 K. Here we focus on the systems with heterogeneous particles consist of one atom and six atoms (Fig. 4(a) and (b), respectively). For a comparison, the system with uniform interface intermixing (no composition grading) is also studied. In general, the investigated systems exhibit similar behavior: the phonon transmission decreases with L for most of the frequencies. A lower phonon transmission indicates more hindrance in thermal transport, which is in accordance with the L-dependent thermal conductivity shown in Fig. 3. The ballistic transport can be observed below ~1 THz for the composition graded structures, where the transmission is insensitive to L.

For higher frequencies, the crossover from the ballistic to the diffusive regime is expected to occur, where a power law decay with composition grading length ($T(\omega) \propto L^{-1}$) should be observed [29]. As L increases, the heterogeneous particles-induced backscattering effects may become increasingly important, and the localization regime can be established, featured by the exponential decay of phonon transmission [30] as $T(\omega) \propto e^{-L/\xi}$. Here ξ denotes the phonon localization length, which indicates the typical length needed for the occurrence of phonon localization in disordered systems. Phonon localization has been previously observed in graphene-based systems such as amorphous graphene [31], disordered graphene phononic crystals [32] and graphene nanomesh [33], etc. It was also found in silicon nanowires [34,35]. To identify the phonon suppressing mechanism in our systems, we fit $T(\omega)$ with both power law decay (Eq. (6)) and exponential decay ((Eq. (7)) with different L for each frequency:

$$T(\omega) = A \cdot L^{-1}, \tag{6}$$

$$T(\omega) = T_0(\omega) \cdot e^{-L/\xi}, \tag{7}$$

where A is a fitting parameter, and $T_0(\omega)$ is the phonon transmission coefficient of the structure with abrupt interface. We used the coefficient of determination, R^2, to evaluate the goodness of the fit [36]. An R^2 of 1 indicates that the model perfectly fits the data.

Interestingly, fitting $T(\omega)$ to Eq. (6) gives low values of R^2 (below 0.7) over the whole frequency range of the three structures, suggesting that the diffusive regime in our structures is not distinct and phonon mean free paths (l_{mfp}) and ξ are not well-separated. In contrast, fitting $T(\omega)$ to Eq. (7) can give very high values of R^2, depending on the frequency, which provides the evidence of Anderson localization for the modes of these frequencies. From the well-fitted curves ($R^2 \geqslant 0.96$), we can obtain the frequency dependent phonon localization length, as plotted in Fig. 5(a). It can be clearly seen that more phonon modes (especially with frequencies below 10 THz) are localized in the models with composition-graded interfaces, with respect to the one with uniform intermixing section. It also shows that larger scatter size (larger heterogeneous particle) traps more phonons due to Anderson localization.

Anderson localization for a certain phonon frequency will happen only if incoherent effects are weak. At higher temperatures where the anharmonic relaxation length (l_ϕ) is comparable to or smaller than the localization length (i.e. $l_\phi \leqslant \xi$), the localization effects will not take place. In other words, the anharmonicity will destroy phonon localization at elevated temperatures [37,38]. To gain more insights, we calculated ξ at higher temperatures (500 K and 800 K), and the results are shown in Fig. 5(b), (c) and (d). Indeed, for all the three models, the population of localized modes obviously decreases with temperature, over the whole frequency range.

From the L-dependent phonon transmission spectra, we evaluated the frequency resolved l_{mfp} [39] from the relationship $T(\omega) = N(\omega)\left(1 + \frac{L}{l_{mfp}}\right)^{-1}$, where $N(\omega)$ is the number of phonon modes at a given frequency in pure graphene. The calculated l_{mfp} for the model with 6-atom heterogeneous particles and the one with abrupt interface are plotted in Fig. 6(a). Also plotted is the anharmonic relaxation length (l_ϕ) in graphite materials, which is roughly estimated [40] from $l_\phi = BT^{-1}\omega^{-2}, B = 3.35 \times 10^{23}$ mKs^{-2}. As revealed in Fig. 6(a), l_{mfp} of Gr/h-BN lateral heterostructure decreases with composition diffusion width, which complies with our thermal conductivity calculations. l_ϕ is estimated to be orders of magnitude larger than l_{mfp} in Gr/h-BN lateral heterostructures, which confirms that the incoherent effects are weak in our systems at 300 K.

In addition, we calculated the Thouless length [41,42] $\xi' = N(\omega) l_{mfp}$, which is a crude estimation of the localization length. According to Fig. 6(b), ξ' is larger than ξ, suggesting that the Thouless relation does not hold in our case. There are two possible reasons for this discrepancy: firstly, the Thouless relation is under the assumptions of weak disorder and isotropic scattering. Our systems with interface diffusion has an anisotropic feature in composition through the graded interface, which may cause anisotropic scattering. Secondly, the Thouless relation requires the diffusive and localized regimes are clearly separated [43]. However, the failure of fitting $T(\omega)$ to Eq. (6) ($R^2 \leqslant 0.7$) indicates that the diffusive regime in our particular system is indistinct, thus the separation of transport regimes is not so clear-cut. The relatively small number of transport channels ($N(\omega) \sim 20$) also verifies this argument.

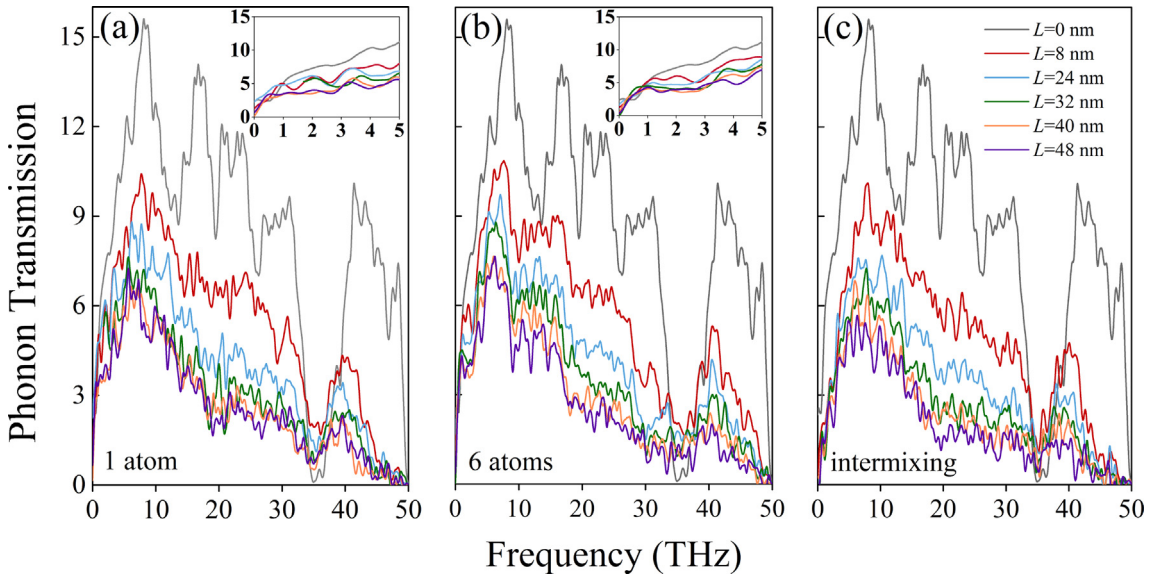

Fig. 4. *L*-dependent phonon transmission spectra of composition graded Gr/h-BN with heterogeneous particles consist (a) one atom and (b) six atoms, and (c) Gr/h-BN with uniform interface intermixing.

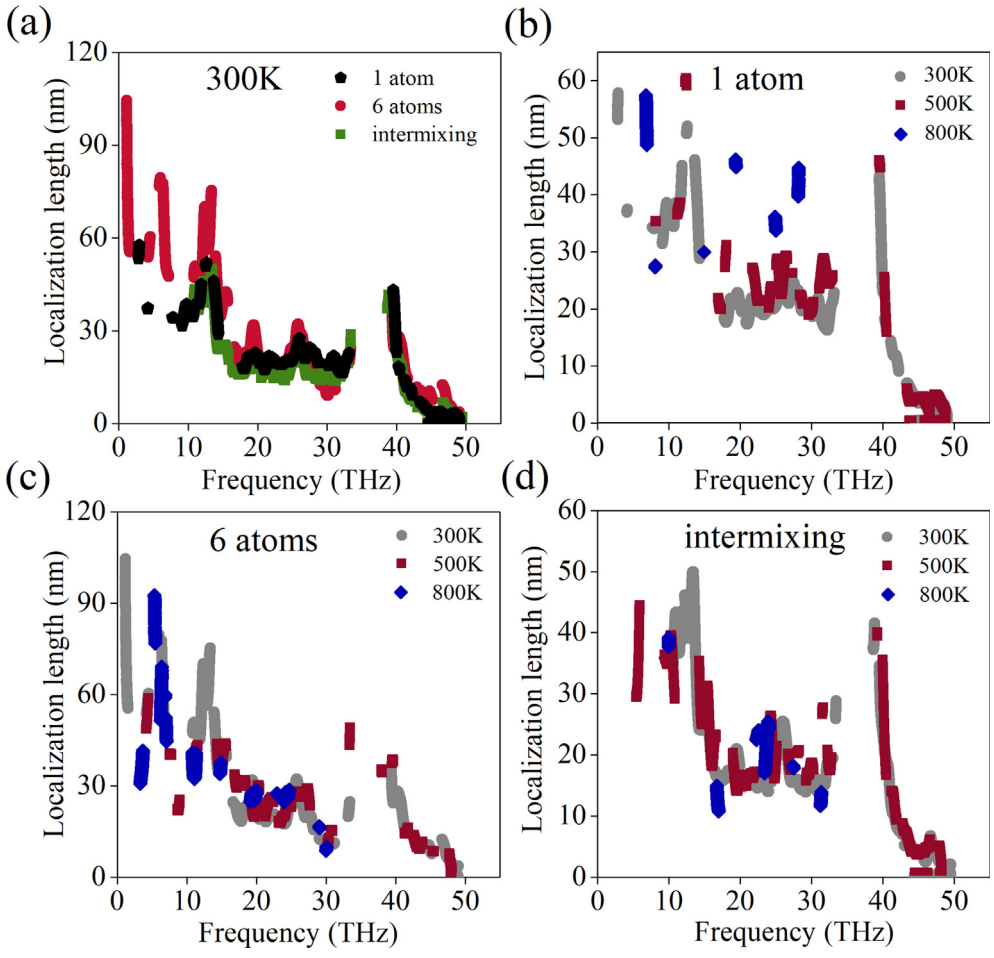

Fig. 5. Phonon localization length of different models at different temperatures.

Fig. 6(b) indicates that the phonon mean free path dramatically decreases with the frequency (almost one order of magnitude in the frequency rang ⩽10 THz), due to the significant decrease of the phonon wavelength as frequency increases. On the other hand, the phonon localization length does not decrease too much. This sugests that, in this frequency range, the typical length needed

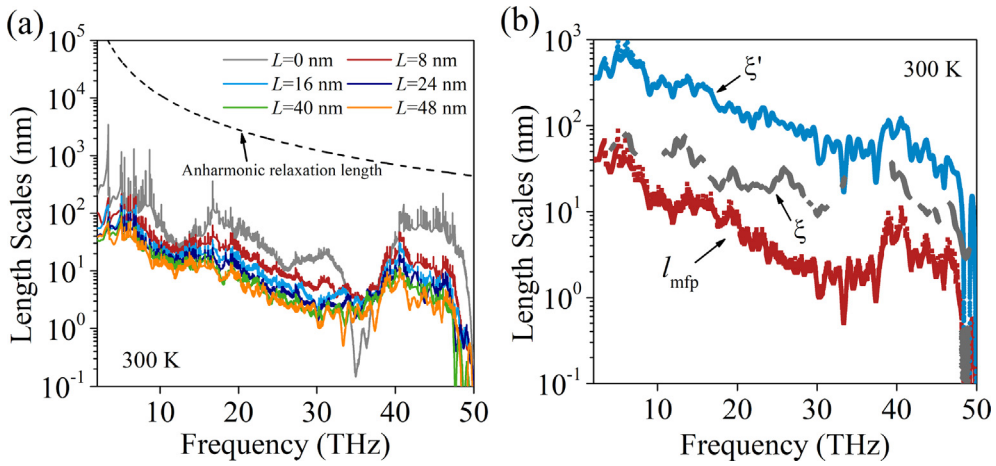

Fig. 6. (a) Phonon mean free path of Gr/h-BN heterostructures with different L. The black dashed line denotes the anharmonic relaxation length in graphite materials. (b) A comparison of the phonon mean free path, localization length ξ and Thouless length ξ' for the model with L = 48 nm at 300 K.

for the occurrence of phonon localization in the systems under investigation remains in the length scale of tens of nanometers, which is not quite affected by the phonon frequency.

The interface roughness is reported to slightly increase the interface thermal conductance by changing the contact area [44–46]. It is interesting to note that the interface diffusion introduces disorders over large spatial extent (to tens of nanometers) around the interface rather than local topography change, which severelly scatters phonons over the whole disordered structure.

4. Conclusions

In summary, we report that the thermal conductivity of graphene/h-BN lateral heterostructures is largely dependent on the structure of the interfaces. Our molecular dynamics simulations show that the length of the interface composition diffusion can be used to tune the thermal conductivity of the heterostructures. The analyses of phonon transmission function prove the existence of the localized phonons, which is identified to be the primary cause of the phonon suppressing. Phase breaking interactions are shown to delocalize the modes at elevated temperatures due to the increased anharmonicities. This work suggests that the interface formation of 2D lateral heterostructures has significant impact on the thermal transport, and nonabrupt, graded interface can be beneficial for their applications in thermoelectrics and thermal insulators, where low thermal conductivity is desired.

Declaration of Competing Interest

The authors declare that they have no conflicts of interest to this work.

Acknowledgment

Y. Ni acknowledges the support of National Natural Science Foundation of China (NSFC) Grant No. 11774294, and the R&D Program for International S&T Cooperation and Exchanges of Sichuan province (Grant No. 2018HH0088). H. Wang acknowledges the Applied Science and Technology Project of Sichuan Province Grant No. 2017JY0056. S. Xiong acknowledges the financial support from National Natural Science Foundation of China (Grant No. 11804242), and the Jiangsu Provincial Natural Science Foundation (Grant No. BK20160308). This work is supported by the Doctoral Innovation Fund Program of Southwest Jiaotong University.

References

[1] H. Wang, F. Liu, W. Fu, Z. Fang, W. Zhou, Z. Liu, Two-dimensional heterostructures: fabrication, characterization, and application, Nanoscale 6 (21) (2014) 12250–12272.
[2] L. Liu, J. Park, D.A. Siegel, K.F. Mccarty, K. Clark, W. Deng, L. Basile, J.C. Idrobo, A. Li, G. Gu, Heteroepitaxial growth of two-dimensional hexagonal boron nitride templated by graphene edges, Science 343 (6167) (2014) 163–167.
[3] Q. Li, M. Liu, Y. Zhang, Z. Liu, Hexagonal boron nitride-graphene heterostructures: Synthesis and interfacial properties, Small 12 (1) (2016) 32–50.
[4] P. Sutter, R. Cortes, J. Lahiri, E. Sutter, Interface formation in monolayer graphene-boron nitride heterostructures, Nano Lett. 12 (9) (2012) 4869–4874.
[5] L. Zheng, L. Ma, S. Gang, Z. Wu, Y. Gong, S. Lei, X. Yang, J. Zhang, J. Yu, K.P. Hackenberg, et al., In-plane heterostructures of graphene and hexagonal boron nitride with controlled domain sizes, Nat. Nanotechnol. 8 (2) (2013) 119–124.
[6] M. Levendorf, C. Kim, L. Brown, P.Y. Huang, R.W. Havener, D.A. Muller, J. Park, Graphene and boron nitride lateral heterostructures for atomically thin circuitry, Nature 488 (7413) (2012) 627–632.
[7] X. Duan, C. Wang, J.C. Shaw, R. Cheng, Y. Chen, H. Li, X. Wu, Y. Tang, Q. Zhang, A. Pan, et al., Lateral epitaxial growth of two-dimensional layered semiconductor heterojunctions, Nat. Nanotechnol. 9 (12) (2014) 1024–1030.
[8] Y. Gong, J. Lin, X. Wang, G. Shi, S. Lei, Z. Lin, X. Zou, G. Ye, R. Vajtai, B.I. Yakobson, et al., Vertical and in-plane heterostructures from ws2/mos2 monolayers, Nat. Mater. 13 (12) (2014) 1135–1142.
[9] Y. Gao, Y. Zhang, P. Chen, Y. Li, M. Liu, T. Gao, D. Ma, Y. Chen, Z. Cheng, X. Qiu, et al., Toward single-layer uniform hexagonal boron nitride-graphene patchworks with zigzag linking edges, Nano Lett. 13 (7) (2013) 3439–3443.
[10] G.H. Han, J.A. Rodriguezmanzo, C. Lee, N.J. Kybert, M.B. Lerner, Z.J. Qi, E.N. Dattoli, A.M. Rappe, M. Drndic, A.T.C. Johnson, Continuous growth of hexagonal graphene and boron nitride in-plane heterostructures by atmospheric pressure chemical vapor deposition, ACS Nano 7 (11) (2013) 10129–10138.
[11] J. Lu, K. Zhang, X. Liu, H. Zhang, T.C. Sum, A.H.C. Neto, K.P. Loh, Order-disorder transition in a two-dimensional boron-carbon-nitride alloy, Nat. Commun. 4 (2013) 2681.
[12] T. Gao, X. Song, H. Du, Y. Nie, Y. Chen, Q. Ji, J. Sun, Y. Yang, Y. Zhang, Z. Liu, Temperature-triggered chemical switching growth of in-plane and vertically stacked graphene-boron nitride heterostructures, Nat. Commun. 6 (1) (2015) 6835.
[13] J. Lu, L.C. Gomes, R.W. Nunes, A.H.C. Neto, K.P. Loh, Lattice relaxation at the interface of two-dimensional crystals: Graphene and hexagonal boron-nitride, Nano Lett. 14 (9) (2014) 5133–5139.
[14] M. Mahjourisamani, M. Lin, K. Wang, A.R. Lupini, J. Lee, L. Basile, A. Boulesbaa, C.M. Rouleau, A.A. Puretzky, I.N. Ivanov, et al., Patterned arrays of lateral heterojunctions within monolayer two-dimensional semiconductors, Nat. Commun. 6 (1) (2015) 7749.
[15] Y. Han, M. Li, G.S. Jung, M.A. Marsalis, Z. Qin, M.J. Buehler, L. Li, D.A. Muller, Sub-nanometre channels embedded in two-dimensional materials, Nat. Mater. 17 (2) (2017) 129–133.
[16] J. Zhang, Y. Hong, Y. Yue, Thermal transport across graphene and single layer hexagonal boron nitride, J. Appl. Phys. 117 (13) (2015) 134307.
[17] Y. Hong, J. Zhang, X.C. Zeng, Thermal contact resistance across a linear heterojunction within a hybrid graphene/hexagonal boron nitride sheet, Phys. Chem. Chem. Phys. 18 (35) (2016) 24164–24170.
[18] See Supplemental Material at [URL will be inserted by publisher] for details of the impact of C—C, B—N bond length mismatch, domain size, correlation length and equilibrium time on the calculated thermal conductivity of graphene/h-BN heterostructures.

[19] A. Kinaci, J.B. Haskins, C. Sevik, T. Cagin, Thermal conductivity of bn-c nanostructures, Phys. Rev. B 86 (11) (2012).
[20] L. Lindsay, D. Broido, Optimized tersoff and brenner empirical potential parameters for lattice dynamics and phonon thermal transport in carbon nanotubes and graphene, Phys. Rev. B 81 (20) (2010).
[21] A.A. Balandin, S. Ghosh, W. Bao, I. Calizo, D. Teweldebrhan, F. Miao, C.N. Lau, Superior thermal conductivity of single-layer graphene, Nano Lett. 8 (3) (2008) 902–907.
[22] S. Ghosh, I. Calizo, D. Teweldebrhan, E.P. Pokatilov, D.L. Nika, A.A. Balandin, W. Bao, F. Miao, C.N. Lau, Extremely high thermal conductivity of graphene: Prospects for thermal management applications in nanoelectronic circuits, Appl. Phys. Lett. 92 (15) (2008) 151911.
[23] C. Sevik, A. Kinaci, J.B. Haskins, A. Mcferrin, Characterization of thermal transport in low-dimensional boron nitride nanostructures, Phys. Rev. B 84 (8) (2011).
[24] R. Kubo, M. Toda, N. Hashitsume, Statistical Physics II: Nonequilibrium stastical Mechanics, Springer-Verlag, 1963.
[25] K. Saaskilahti, J. Oksanen, J. Tulkki, S. Volz, Role of anharmonic phonon scattering in the spectrally decomposed thermal conductance at planar interfaces, Phys. Rev. B 90 (13) (2014) 134312.
[26] K. Saaskilahti, J. Oksanen, S. Volz, J. Tulkki, Frequency-dependent phonon mean free path in carbon nanotubes from nonequilibrium molecular dynamics, Phys. Rev. B 91 (115426) (2015) 1–10.
[27] H. Zhang, H. Han, S. Xiong, H. Wang, S. Volz, Y. Ni, Impeded thermal transport in composition graded sige nanowires, Appl. Phys. Lett. 111 (12) (2017) 121907.
[28] H. Sevincli, W. Li, N. Mingo, G. Cuniberti, S. Roche, Effects of domains in phonon conduction through hybrid boron nitride and graphene sheets, Phys. Rev. B 84 (20) (2011).
[29] I. Savi?, N. Mingo, D.A. Stewart, Phonon transport in isotope-disordered carbon and boron-nitride nanotubes: Is localization observable?, Phys Rev. Lett. 101 (16) (2008) 165502.
[30] J.M. Mendoza, G. Chen, Anderson localization of thermal phonons leads to a thermal conductivity maximum, Nano Lett. 16 (12) (2016) 7616–7620.
[31] T. Zhu, E. Ertekin, Phonons, localization, and thermal conductivity of diamond nanothreads and amorphous graphene, Nano Lett. 16 (8) (2016) 4763–4772.
[32] S. Hu, Z. Zhang, P. Jiang, J. Chen, S. Volz, M. Nomura, B. Li, Randomness-induced phonon localization in graphene heat conduction, J. Phys. Chem. Lett. (2018) 3959.
[33] T. Feng, X. Ruan, Ultra-low thermal conductivity in graphene nanomesh, Carbon 101 (2016) 107–113.
[34] D. Ma, H. Ding, H. Meng, L. Feng, W. Yue, J. Shiomi, N. Yang, Nano-cross-junction effect on phonons in silicon-nanowire-cages, Phys. Rev. B 94 (16) (2016) 165434.
[35] D. Ma, A. Arora, S. Deng, G. Xie, J. Shiomi, N. Yang, Quantifying phonon particle and wave transport in silicon nanophononic metamaterial with cross junction, Mater. Today Phys. 8 (2019) 56–61.
[36] N.J.D. Nagelkerke, A note on a general definition of the coefficient of determination, Biometrika 78 (3) (1991) 691–692.
[37] Y. Liu, D. He, Anomalous interfacial temperature profile induced by phonon localization, Phys. Rev. E 96 (6) (2017).
[38] Y. Wang, H. Huang, X. Ruan, Decomposition of coherent and incoherent phonon conduction in superlattices and random multilayers, Phys. Rev. B 90 (16) (2014) 165406.
[39] S. Datta, Electronic Transport in Mesoscopic Systems, Cambridge University Press, 1995.
[40] P.G. Klemens, D.F. Pedraza, Thermal conductivity of graphite in the basal plane, Carbon 32 (4) (1994) 735–741.
[41] D.J. Thouless, Maximum metallic resistance in thin wires, Phys. Rev. Lett. 39 (18) (1977) 1167–1169.
[42] P.W. Anderson, D.J. Thouless, E. Abrahams, D.S. Fisher, New method for a scaling theory of localization, Phys. Rev. B 22 (8) (1980) 3519–3526.
[43] C.W.J. Beenakker, Random-matrix theory of quantum transport, Rev. Mod. Phys. 69 (3) (1997) 731–808.
[44] F. Liu, R. Zou, N. Hu, H. Ning, C. Yan, Y. Liu, L. Wu, F. Mo, S. Fu, Enhancement of thermal energy transport across the graphene/h-bn heterostructure interface, Nanoscale 11 (9) (2019) 4067–4072.
[45] S. Merabia, K. Termentzidis, Thermal boundary conductance across rough interfaces probed by molecular dynamics, Phys. Rev. B. 89 (5) (2014) 054309.
[46] Y. Zhang, D. Ma, Z. Yi, N. Yang, A modified theoretical model to predict the thermal interface conductance considering interface roughness, Front. Energy Res. 6 (48) (2018) 1–6.